AIP Advances

Patterning of graphite nanocones for broadband solar spectrum absorption

Yaoran Sun, Julian Evans, Fei Ding, Shaowei Wang, Lei Mo, and Sailing He

Citation: AIP Advances **5**, 067139 (2015); doi: 10.1063/1.4922894
View online: http://dx.doi.org/10.1063/1.4922894
View Table of Contents: http://scitation.aip.org/content/aip/journal/adva/5/6?ver=pdfcov
Published by the AIP Publishing

Patterning of graphite nanocones for broadband solar spectrum absorption

Yaoran Sun,[1] Julian Evans,[1] Fei Ding,[1] Shaowei Wang,[1] Lei Mo,[1] and Sailing He[1,2,a]

[1]*Centre for Optical and Electromagnetic Research, Zhejiang Provincial Key Laboratory for Sensing Technologies, Zhejiang University, Hangzhou 310058, People's Republic of China*
[2]*Department of Electromagnetic Engineering, Royal Institute of Technology, S-100 44 Stockholm, Sweden*

(Received 31 December 2014; accepted 9 June 2015; published online 19 June 2015)

We experimentally demonstrate a broadband vis-NIR absorber consisting of 300-400 nm nanocone structures on highly oriented pyrolytic graphite. The nanocone structures are fabricated through simple nanoparticle lithography process and analyzed with three-dimensional finite-difference time-domain methods. The measured absorption reaches an average level of above 95% over almost the entire solar spectrum and agrees well with the simulation. Our simple process offers a promising material for solar-thermal devices. [http://dx.doi.org/10.1063/1.4922894]

Efficient absorption of light is increasingly important in many fields of science and technologies, such as solar thermoelectric generators, solar thermophotovoltaic devices, controllable thermal emission, and sensing.[1–4] Graphite, a naturally black material with a relatively large imaginary part of refractive index over a large spectral range from visible to infrared light,[5] is a practical material choice for broadband absorber design. Almost perfect light absorption can be achieved in a very wide spectral range (0.2-200 um) by vertically aligned carbon nanotube array materials.[6] However, this is generally at the cost of the structural thickness (several tens to hundreds micrometer) due to the relatively low material density (~3% of bulk graphite).[6,7] Meanwhile, metamaterial inspired nanostructures can realize broadband absorption by optically thin designs.[8–10] However, such approaches require complicated nanofabrication including electron beam lithography or focused ion beam milling, which are time-consuming, and not scalable.

Previous studies have shown that the modification of the surface of highly oriented pyrolytic graphite (HOPG) with pillar-like or disk-like nanostructures can enhance its optical absorption.[11,12] However, only moderate absorptivities (~85%) within relatively narrow bandwidths at visible spectra have been realized. Here we report that polyethylene glycol (PEG) capped gold nanoparticles (GNPs) and optimized plasma etching conditions can produce nanocone structures that cover the vast majority of the surface area allowing for average reflection coefficients below 5% in a broad wavelength range of 450-1800 nm. Owing to its large imaginary part of refractive index, this HOPG absorber can efficiently absorb the energy of broadband light in a thin film of around 1 μm, which is comparable to metamaterial inspired devices.

The absorber is composed of randomly distributed HOPG cone structures with feature sizes of few-hundred nanometers on top of bulk HOPG substrate as schematically shown in Fig. 1(a). Tilted view scanning electron microscopy (SEM) picture of the fabricated sample etched out from bulk HOPG material shows closely packed, randomly distributed nanocones at the surface [Fig. 1(b)].

The fabrication process for HOPG nanocone structures is simply spin-coating GNPs, etching, and washing away the mask as schematically shown in Fig. 2(a). We synthesize GNPs using a

[a]sailing@kth.se

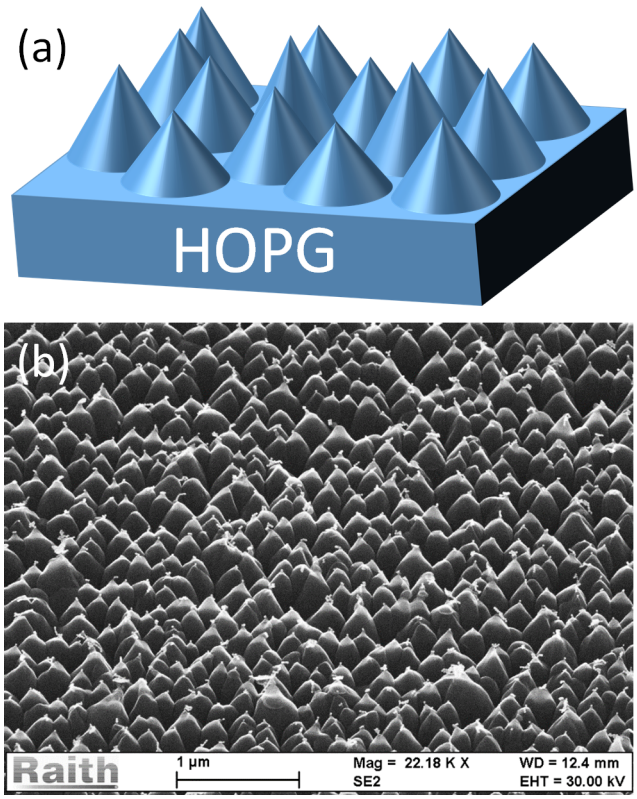

FIG. 1. (a) Schematic of proposed HOPG nanocone structures; (b) tilted view SEM picture of the fabricated sample with GNPs on the top of each nanocone.

modified seed-mediated method.[13] Transmission electron microscopy (TEM) of the as-prepared GNPs shows that the GNPs have diameters around 25 nm and the shapes are mostly spheres with a small proportion of triangles [Fig. 2(b)]. The as-prepared GNPs are then recapped with methoxy polyethyleneglycol thiol (mPEG-SH, MW5000, JenKem Technology Co., Ltd.) in water according to the procedure described in Ref. 14 with minor modifications. After being sedimented by

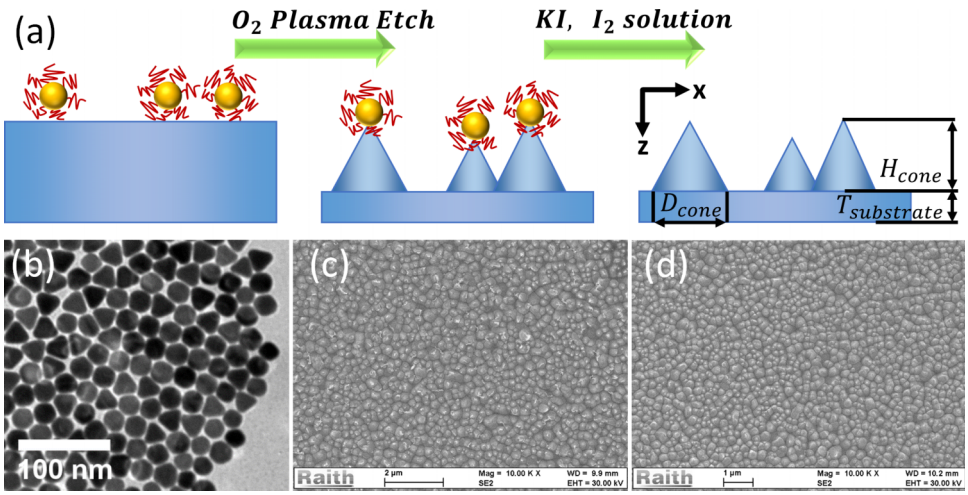

FIG. 2. (a) Flow chart of the fabrication of nanocone structures (b) TEM picture of the as-prepared GNPs. Top view SEM pictures of the fabricated sample before (c) and after (d) the GNPs are etched and washed off.

centrifugation at 8000 rpm for 10 minutes, the solvent of GNPs solution is replaced by ethanol. We repeat this process 3 times to remove the water residue and then concentrate the solution to have a final concentration 140 times that of an optical density 1 solution or "linear" optical density (lOD) of 140 at λ = 535 nm, measured by Shimadzu 2550 UV-Vis scanning spectrophotometer. We spin coat this GNPs solution on a freshly peeled HOPG ($5 \times 5 \times 1$ mm, B class, Nanjing XFNANO Materials Tech Co., Ltd.) surface at the speed of 4000 rpm for 60 seconds to form the desired particle density. The area density of GNPs at the central region of the HOPG sample is found to be around 15 particles/μm^2 with a few dimer or trimer aggregates. The HOPG sample is subsequently loaded into an inductively coupled plasma (ICP) system for a 2 minutes oxygen based plasma etching to remove the carbon atoms not shadowed by the GNPs.[11,12,15,16] By tuning the etching conditions (powers and oxygen pressure), cone structures with different sidewall angles could be produced. In our experiments, an optimized etching condition (45 W platen power, 800 W coil power, 20 mTorr, 90 sccm) is used to fabricate the nanocone structures for the absorber device. As shown in a top view SEM picture in Fig. 2(c), the sizes of GNPs are found well maintained, showing that the GNPs are robust for working as the etch masks. The base diameters of the nanocones are defined by both their distances to adjacent GNPs and the etching time, and the height to base diameter ratio is controlled by the sidewall angle. A 2-minute ICP etch process is sufficient to achieve a nanocone coverage above 90% for the structural density around 12 cones/μm^2. With such high structural coverage, the nanocone structures will dominate the absorption of this device. Wet etching the sample in an iodine-based gold etch (4 g KI, 1 g I_2, 80 mL DI water) for 20 minutes removes the GNPs from the substrate. Finally, we wash the sample several times with DI water. A top view SEM picture of the final HOPG absorber sample in Fig. 2(d) shows that the HOPG structures are not affected by the wet etching process.

In order to map the cross section profiles of these nanocones, an HOPG sample with lower area density and thinner substrate (around 200 μm) is prepared using the same procedure with a GNPs solution having an lOD of 20 for the etch mask spin-coating. Since thin layers of HOPG are bendable, a side view of the cones could be achieved by simply curling the sample attached to tape without destroying the structures. A side view with a slight tilt angle and a top view SEM pictures of this low-density sample are presented in Fig. 3(a) and 3(b), respectively. For most nanocone structures, their heights and base diameters fall in the range of 300 to 400 nm. In the regions not covered by the nanocones, relatively flat surfaces with features smaller than 50 nm show good etching quality.

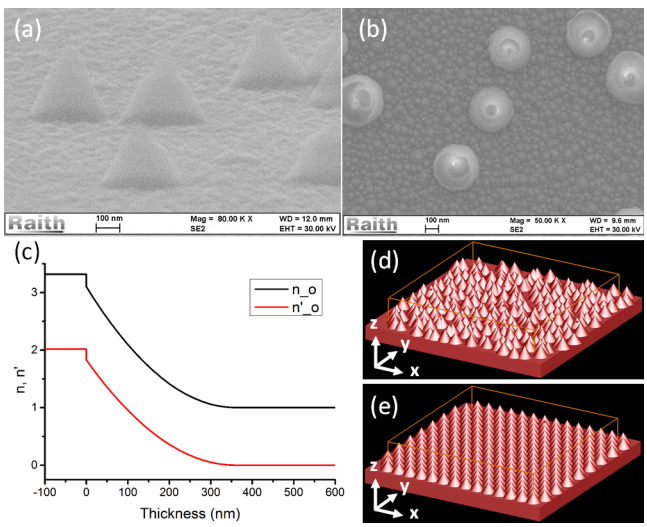

FIG. 3. Side view with slight tilt angle (a) and top view (b) SEM of sparsely distributed nanocones; (c) the real and imaginary parts of the effective refractive index profiles of the 90% covered model with 360 nm-nanocones for ordinarily polarized light; schematics of the randomized model with random nanocone sizes (d) and the periodic model with hexagonally patterned nanocones with uniform height and base diameter of 360 nm (e).

Based on the nanocone structure parameter extracted from the low-density sample, we calculate the effective refractive indices profiles by averaging the real part and imaginary part of the refractive index of air ($n_{air} = 1, n'_{air} = 0$) and graphite ($n_{graphite\_o} = 3.316$, $n'_{graphite\_o} = 2.017$) for ordinarily polarized light at $\lambda = 1127$ nm weighted by volume at different heights,[17] assuming 90% surface of the model is covered by 360-nm nanocones (nanocones with both the heights and base diameters to be 360 nm). Because the sizes of our interested structures are mainly on the scale of few hundreds of nanometers, in this article, we take dispersive optical constants for HOPG within the vis-NIR range from Ref. 18, which characterizes the optical responses for both ordinary and extraordinary incident light for graphite grain with 100 nm radius. As shown in Fig. 3(c), the calculated effective refractive index gradually decreases from the bottom part to the top part of the model, thus providing impedance match between the HOPG substrate and the air. After impinging on the structure, light can be easily coupled into the HOPG nanocones due to impedance match.

Numerical simulations of nanocone structure models with different sizes and packing styles are performed using three-dimensional (3D) finite-difference time-domain (FDTD) methods (Lumerical FDTD Solutions). We build models composed of randomly distributed nanocones mimicking the fabricated sample and a periodic model composed of hexagonally patterned nanocones, as shown in Fig. 3(d) and 3(e), respectively. In both models, we define the simulation in a 4 μm × 4 μm area (the regions in the orange boxes) with periodic boundary conditions in the x and y directions. In the randomized models, the positions of the nanocones are randomly generated by the embedded script language of the Lumerical FDTD Solution software. While in the periodic model, 195 (around 12.2 cones/μm^2) nanocones of base diameter and height of 360 nm are closely placed on a 15×13 hexagonal lattice. Under the nanocones, the 500 nm thick HOPG substrate is also included in our simulations to block all light transmission. In the simulations, a plane wave of TE polarization (electric field is polarized along the x-axis) impinges on the structure normally along the negative direction of z-axis as the excitation source.

Reflection spectra of the fabricated sample are studied using a homemade reflection spectroscopy[10] in the wavelength range of 450-1800 nm. The sample is illuminated by a halogen lamp under Kohler condition through a 60× objective (N.A = 0.85). The reflected light is collected in the backscattering configuration by the same objective. The large numerical aperture of the objective is used to collect most of the reflected light. Far field simulations of the randomized models indicate that around 90% of all reflected light will be captured by this large N.A. lens, indicating that this is a reasonable method to characterize the material. A tunable square aperture with side length of 1.5 mm is set at the conjugate plane of the sample to control the image area with a side length of 25 μm. In this way, we can make sure that the backscattering light collected is mainly from the central area of the sample and thereby suppress the background noise. The signal of visible wavelength (450-800 nm) is measured directly by using an Ocean Optics USB2000 spectrometer that is controlled by a computer. For the signal of long wavelength (800-1800 nm), a monochrometer (Zolix, Omni-λ1509) is used in combination with an infrared InGaAs detector, also working in a remote operational mode. Reflectivity spectra are obtained by using calibration reflection measurements with a reference aluminum mirror. Because of the cylindrical symmetry of the elementary structures and the random distribution, our absorber is naturally polarization independent. Thus unpolarized light is used as the excitation source.

In both experimental and simulated results, the absorption is defined as $A(\lambda) = 1 - R(\lambda) - T(\lambda)$, where $T(\lambda)$ and $R(\lambda)$ are the total transmission and reflection respectively. Since the bottom HOPG is thick enough to block all the transmitted light, there is zero transmission, consequently the absorption can be simply given by $A(\lambda) = 1 - R(\lambda)$. The measured absorption of the fabricated sample, the HOPG surface roughened up by abrasive paper (Silicon Carbide, Cw 400) and the flat HOPG surface are presented along with the 3D FDTD simulated absorption of a randomized model in Fig. 4(a). This model has random heights and base diameters in the range of 320-400 nm and a nanocone density of around 12.2 cones/μm^2. Since the HOPG surface roughened by abrasive paper is nonuniform, we have randomly chosen 5 regions for this measurement, and the result shown here is the average of those 5 measurements. Note that the discontinuity of the measured curves at wavelength $\lambda = 800$ nm is due to the high noise level of InGaAs detector at the short wavelength region, and it is not an intrinsic property of the samples. The measured result of the fabricated sample

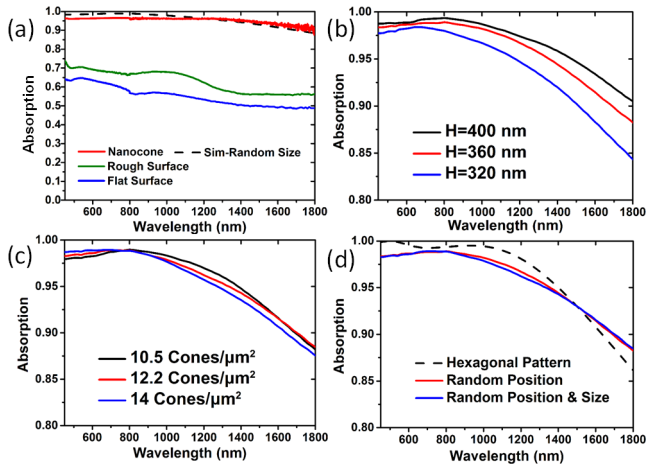

FIG. 4. (a) The measured absorption spectra of the fabricated HOPG nanocone absorber (red solid line), the HOPG surface roughened by abrasive paper (green solid line), the flat HOPG surface (blue solid line), along with the simulated absorption spectrum of the randomized model with random heights and base diameters in the range of 320-400 nm (black dashed line). Comparisons of simulated absorption spectra of the randomized models with different heights (b), nanocone densities (c), and structure randomness (d), respectively.

shows an excellent absorption performance, with absorptivity higher than 96% covering the wavelength range from 450 nm to 1200 nm, reaching an average level of above 95% over the measured spectrum range. Compared with the HOPG surface roughened by abrasive paper and the flat HOPG surface, the HOPG surface modified by nanocone structures shows significantly enhanced absorption in the measured spectrum range. Compared with HOPG surfaces modified with nanopillars and nanodisks in previous studies,[11,12] our sample shows a much higher peak absorptivity and much wider absorbing bandwidth. The experimental data agrees well with the simulated spectrum on the overall absorption level except some deviation at the short and long wavelength ends.

Further numerical studies about the dependence of absorption on the geometry parameters of randomly packed HOPG nanocones are presented in Fig. 4(b)-4(d). From Fig. 4(b), it is clearly seen that the higher nanocone structure increases the absorption efficiency over the entire wavelength range of 450-1800 nm when the base diameter (360 nm) and the nanocone density (12.2 cones/μm^2) are fixed. Higher nanocone leads to a smoother profile of the effective refractive index at the air-nanocone and nanocone-HOPG substrate interfaces, thus decreasing the reflection further. On the other hand, shorter nanocones result in a higher reflection due to abrupt effective refractive index change.

To verify the influence of the nanocone densities, simulations of three randomized models composed of 360-nm nanocones are performed. In these models, 168, 195, and 224 nanocones are randomly distributed, corresponding to the nanocone densities of 10.5, 12.2 and 14 cones/μm^2 respectively. As the nanocone density decreases, the absorption at short wavelength below 800 nm decreases, while the absorption at long wavelength increases.

Fig. 4(d) compares models with different structure randomness with fixed nanocone density (12.2 cones/μm^2). The black dashed line corresponds to the periodic model with hexagonally patterned 360-nm nanocones depicted in Fig. 3(e). The red solid line shows the absorption spectrum of the randomized model composed of 360-nm nanocones, while the blue solid line plots the absorption spectrum of randomized model with random nanocone heights and base diameters ranging from 320 to 400 nm. The 2 solid lines almost coincides with each other, shows the averaging effect of the absorptions of nanocones with different sizes. Compared with the periodic model, the absorption spectra of the randomized models are lower at wavelengths below λ = 1400 nm and higher at longer wavelengths. Since the Bloch modes associated with the periodicity are absent in the randomized models, their absorption curves are relatively smooth, as observed in the measured result. These simulation results clearly show that height is the critical parameter for achieving high absorption.

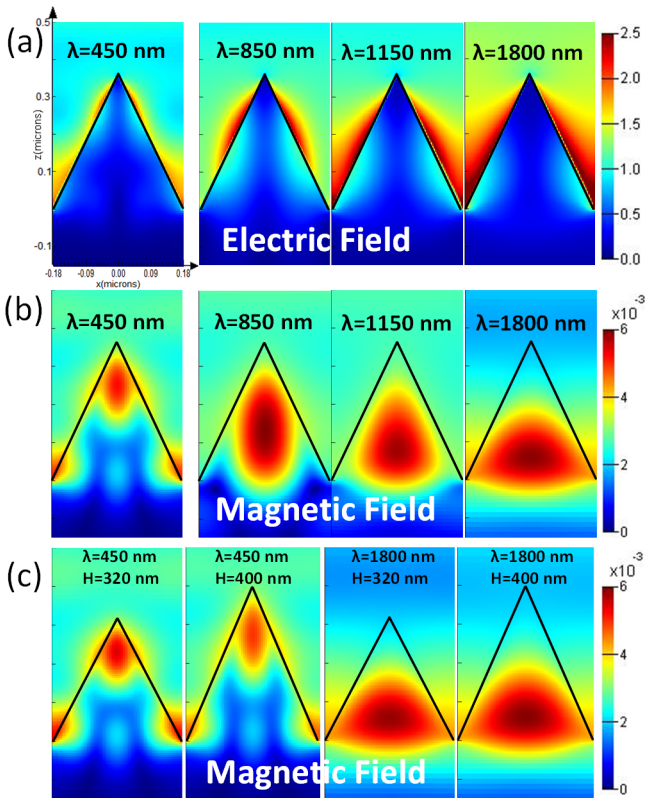

FIG. 5. Electric (a) and magnetic (b) field distributions in $x-z$ plane of the 360 nm-nanocone model at different wavelengths; (c) magnetic field distributions in $x-z$ plane of the nanocone models with heights of 320 and 400 nm at wavelengths of 450 and 1800 nm.

The electric [Fig. 5(a)] and magnetic [Fig. 5(b)] field distributions in the x-z cross-section at different wavelengths are calculated for the 360 nm-nanocone structure with normally incident TE-polarized light. The wavelength-dependent fundamental TE modes can be clearly seen. The modes of shorter wavelengths are excited at upper part of the cone, where the structure is narrower. We observe minor irregularities in the formation of the tips [fig. 1(b)] and the dispersive optical constants we chose are not necessarily correct for regions much narrower or wider than 100 nm, so this potentially accounts for some of the discrepancies between the measured and simulated spectra in the short and long wavelength ranges.

The magnetic field distributions of nanocone structures with different heights (320 and 400 nm) and same base diameter (360 nm) are compared for wavelength $\lambda = 450$ and 1800 nm for TE polarization. As shown in Fig. 5(c), the field distributions in higher nanocones have almost identical patterns as those in shorter nanocones, except that they are stretched along within the cone structures in the z-direction, resulting in a larger light-mater interaction area. This agrees with our observation in Fig. 4(b) that higher nanocones have larger absorptions over the entire simulated spectrum while the absorption curves for structures with different heights have similar shapes.

Since HOPG has large in-plane thermal conductivity (~2000 W mK^{-1} at room temperature),[19] and the HOPG nanocone absorber can potentially be produced as thin as around 1 μm, high thermal conduction efficiency could be achieved when integrated with other components. Moreover, HOPG has high melting point (>3000K),[20] makes it a practical material choice for the absorber working in high temperature environments.[1,2]

In conclusion, we have demonstrated a broadband absorber that performs well (with average absorption above 95%) for the vast majority of the solar spectrum. Given the high wettability of the used gold nanospheres, such a technology could potentially be developed for a roll-to-roll application. This bendable, thermally conductive, absorbing material has promising applications in flexible

thermal photonic devices. Furthermore, graphite is stable at very high temperatures so this could be a useful substrate for the collector at a solar concentrating farm.

ACKNOWLEDGEMENTS

The authors acknowledge the support by the National Natural Science Foundation of China (Nos. 91233208 and 61178062), the National High Technology Research and Development Program (863 Program) of China (No. 2012AA030402). Thanks to Shaochuan Wang for assistance on the measurement of the concentration of GNPs.

[1] D. Kraemer, B. Poudel, H. P. Feng, J. C. Cavlor, B. Yu, X. Yan, Y. Ma, X. W. Wang, D. Z. Wang, A. Muto, K. McEnaney, M. Chiesa, Z. F. Ren, and G. Chen, Nature Mater. **10**, 532 (2011).
[2] A. Lenert, D. M. Bierman, Y. Nam, W. R. Chan, I. C. Celanović, M. Soljačić, and E. N Wang, Nature nanotechnology **9**(2), 126 (2014).
[3] E. Rephaeli and S. H. Fan, Opt. Express **17**, 15145 (2009).
[4] S. P. Theocharous, E. Theocharous, and J. H. Lehman, Infrared Physics & Technology **55**, 299 (2012).
[5] Edward D. Palik, *Handbook of Optical Constants of Solids* (Academic press, 1998), Vol. 2, p. 449.
[6] K. Mizuno, J. Ishii, H. Kishida, Y. Hayamizu, S. Yasuda, D. N. Futaba, M. Yumura, and K. Hata, Proc. Natl. Acad. Sci. **106**, 16044 (2009).
[7] X. J. Wang, L. P. Wang, O. S. Adewuyi, B. A. Cola, and Z. M. Zhang, Appl. Phys. Lett. **97**, 163116 (2010).
[8] K. Aydin, V. E. Ferry, R. M. Briggs, and H. A. Atwater, Nature Communications **2**, 517 (2011).
[9] M. G. Nielsen, A. Pors, O. Albrektsen, and S. I. Bozhevolnyi, Optics Express **20**, 13311 (2012).
[10] L. Mo, L. Yang, A. Nadzeyka, S. Bauerdick, and S. He, Opt. Express **22**, 32233 (2014).
[11] H. Fredriksson, D. Chakarov, and B. Kasemo, Carbon **47**, 1335 (2009).
[12] H. Fredriksson, T. Pakizeh, M. Kall, B. Kasemo, and D. Chakarov, J. Opt. A: Pure Appl. Opt. **11**, 114022 (2009).
[13] S. Sivapalan, B. DeVetter, T. Yang, M. Schulmerich, R. Bhargava, and C. Murphy, The Journal of Physical Chemistry C **117**(20), 10677 (2013).
[14] S. Wang, W. Xi, F. Cai, X. Zhao, Z. Xu, J. Qian, and S. He, Theramositics **5**(3), 251-266 (2015).
[15] H. Park, S. Choi, S. Lee, and K. H. Koh, Journal of Vacuum Science B **22**, 1290 (2004).
[16] K. Elersic, I. Junkar, M. Modic, R. Zaplotnik, A. Vesel, and U. Cvelbar, Mater. Tehnol. **45**, 233 (2011).
[17] J. Zhu, Z. Yu, G. Burkhard, C. Hsu, S. Connor, Y. Xu, Q. Wang, M. McGehee, S. Fan, and Y. Cui, Nano Lett. **9**, 279–282 (2009).
[18] B. T. Draine, The Astrophysical Journal **598**(2), 1017 (2003).
[19] A. A. Balandin, Nature Mater. **10**, 569 (2011).
[20] A. I. Savvatimskiy, Carbon **43**, 1115 (2005).